4864 *Biochemistry* **2010,** *49,* 4864–4871
DOI: 10.1021/bi100506j

BIOCHEMISTRY
including biophysical chemistry & molecular biology
Article

Soluble Guanylate Cyclase Is Activated Differently by Excess NO and by YC-1: Resonance Raman Spectroscopic Evidence[†]

Mohammed Ibrahim,[‡] Emily R. Derbyshire,[§,⊥] Alexandra V. Soldatova,[‡] Michael A. Marletta,[§,∥] and Thomas G. Spiro*[,‡]

[‡]*Department of Chemistry, University of Washington, Seattle, Washington 98195,* [§]*Department of Molecular and Cell Biology, University of California, Berkeley, California 94720-3220, and* [∥]*Department of Chemistry, University of California, Berkeley, California 94720-3220* [⊥]*Present address: Department of Biological Chemistry and Molecular Pharmacology, Harvard Medical School, Boston, MA 02115.*

Received April 3, 2010; Revised Manuscript Received May 11, 2010

ABSTRACT: Modulation of soluble guanylate cyclase (sGC) activity by nitric oxide (NO) involves two distinct steps. Low-level activation of sGC is achieved by the stoichiometric binding of NO (1-NO) to the heme cofactor, while much higher activation is achieved by the binding of additional NO (xsNO) at a non-heme site. Addition of the allosteric activator YC-1 to the 1-NO form leads to activity comparable to that of the xsNO state. In this study, the mechanisms of sGC activation were investigated using electronic absorption and resonance Raman (RR) spectroscopic methods. RR spectroscopy confirmed that the 1-NO form contains five-coordinate NO-heme and showed that the addition of NO to the 1-NO form has no significant effect on the spectrum. In contrast, addition of YC-1 to either the 1-NO or xsNO forms alters the RR spectrum significantly, indicating a protein-induced change in the heme geometry. This change in the heme geometry was also observed when BAY 41-2272 was added to the xsNO form. Bands assigned to bending and stretching motions of the vinyl and propionate substituents undergo changes in intensity in a pattern suggesting altered tilting of the pyrrole rings to which they are attached. In addition, the N−O stretching frequency increases, with no change in the Fe−NO stretching frequency, an effect modeled via DFT calculations as resulting from a small opening of the Fe−N−O angle. These spectral differences demonstrate different mechanisms of activation by synthetic activators, such as YC-1 and BAY 41-2272, and excess NO.

The gaseous signaling molecule nitric oxide (NO)[1] powerfully modulates a large range of physiological responses (*1*−*3*). In eukaryotes, NO signaling is transduced by the hemoprotein soluble guanylate cyclase (sGC) (*4*) which generates the second messenger cyclic GMP (cGMP) at a rate that is strongly upregulated by NO. cGMP in turn regulates a host of other enzymes, including phosphodiesterases, cGMP-gated ion channels, and cGMP-regulated protein kinases (*4*, *5*).

sGC is a heterodimer consisting of two homologous subunits, α1 and β1. The β1 subunit contains the heme cofactor present within a Heme-Nitric oxide/OXygen binding (H-NOX) domain (*6*). This domain has been localized to the ∼200 N-terminal residues of the β1 subunit and is a conserved heme-binding domain found in prokaryotes and eukaryotes (*7*). NO has long been known to bind the heme prosthetic group of sGC, forming a transient 6-c adduct, which then dissociates the proximal histidine ligand, leaving 5-c NO-heme (*8*, *9*). Formation of the 5-c NO complex has been shown to coincide with increased enzyme activity, suggesting that the histidine dissociation is an integral step in sGC regulation by NO (*9*−*11*). However, it has recently been shown that the Fe−NO adduct formed in the presence of stoichiometric NO (1-NO) is activated only modestly from the basal enzyme rate, while the Fe−NO adduct formed in the presence of excess NO (xsNO) exhibits high activity (*12*, *13*). Experiments conducted with methyl methanethiosulfonate (MMTS) suggest that this second NO binding event involves one or more cysteine residues (*14*). Additionally, the high-activity state is transient and persists under anaerobic conditions, suggesting that the activating species is not a nitrosothiol, but possibly a direct adduct of NO with thiol (*14*).

The low-activity 1-NO adduct can be further activated by the allosteric activator YC-1 3-(5′-hydroxymethyl-3′-furyl)-1-benzylindazole (*13*, *15*). YC-1 was discovered in a pharmaceutical screen searching for molecules that would increase cGMP levels in cellular lysate (*16*). Following characterization of YC-1 activation of sGC, BAY 41-2272 {5-cyclopropyl-2-[1-(2-fluorobenzyl)-1*H*-pyrazolo[3,4-*b*]pyridin-3-yl]pyrimidin-4-ylamine} was synthesized in an effort to improve the solubility and efficacy of YC-1 (*17*). Both compounds weakly activate unligated sGC and synergistically activate the CO- and NO-bound forms of the enzyme (*4*, *18*). Additionally, YC-1 and BAY 41-2272 lead to similar changes in the EPR spectra of the sGC−NO complex (*19*),

[†]This work was supported financially by National Institutes of Health Grants GM033576 (T.G.S.) and GM077365 (M.A.M.).

*To whom correspondence should be addressed. Phone: (206) 685-4964. Fax: (206) 685-8665. E-mail: spiro@chem.washington.edu.

[1]Abbreviations: sGC, soluble guanylate cyclase; NO, nitric oxide; 1-NO, stoichiometric binding of NO; xsNO, excess NO binding; CO, carbon monoxide; YC-1, 3-(5′-hydroxymethyl-3′-furyl)-1-benzylindazole; RR, resonance Raman; cGMP, cyclic guanosine 3′,5′-monophosphate; BAY 41-2272, 5-cyclopropyl-2-[1-(2-fluorobenzyl)-1*H*-pyrazolo-[3,4-*b*]pyridin-3-yl]pyrimidin-4-ylamine; H-NOX, Heme-Nitric oxide/OXygen binding; *Tt*, *Thermoanaerobacter tengcongensis*; HEPES, 4-(2-hydroxyethyl)-1-piperazineethanesulfonic acid; DTT, dithiothreitol; GTP, guanosine 5′-triphosphate; DMSO, dimethyl sulfoxide; Ti: sapphire, titanium sapphire; Nd:YLF, neodymium-doped yttrium lithium fluoride; CCD, charge-coupled device; WT, wild type; 6-c, six-coordinate; 5-c, five-coordinate; DFT, density functional theory; PDB, Protein Data Bank.

 Published on Web 05/11/2010

indicating that they induce a similar structural change in the protein and likely bind to the same site. While the exact binding site of these molecules is unknown, there is evidence that they bind to the N-terminus of the α1 subunit (*20*). To date, no endogenously produced sGC activators have been found; however, it remains an intriguing possibility that there may be endogenous small molecules that mediate CO as well as NO signaling.

In this work, electronic absorption and resonance Raman (RR) spectroscopic methods have been used to detect changes in the heme environment when the activators are added to sGC. The spectra establish that the proximal His ligand dissociates from the heme in the 1-NO adduct and that the addition of excess NO to the 1-NO adduct has no further effect on the heme structure. This observation indicates that the molecular events that increase cGMP synthesis in response to excess NO do not directly involve the heme. In contrast, YC-1 does cause changes in the heme environment of both the 1-NO and xsNO adducts. While the NO complex remains 5-c, intensity changes of RR bands associated with the heme vinyl and propionate substituents, together with a shift in a porphyrin vibrational frequency, suggest alterations in the heme out-of-plane distortion. In addition, the N−O stretching frequency shifts in a direction that suggests the Fe−N−O angle opens upon YC-1 binding. These effects point to protein-induced heme alteration associated with YC-1 binding, and its mechanism of activation is clearly different from that of xsNO. Thus, sGC has alternative routes for achieving high activity levels.

EXPERIMENTAL PROCEDURES

Protein Expression, Purification, and Activity Assays. Rat sGC α1β1 was purified as described previously (*21*). Rat β1(1−194) and β1(1−385) were purified according to a previously published protocol (*22*). The β1(1−194) mutants Pro118Ala (P118A) and Ile145Tyr (I145Y) were generated and purified by a method that will be described elsewhere. Additionally, β1(1−194) P118A was purified without heme and reconstituted according to a method that will be described elsewhere.

The 1-NO and xsNO sGC forms were assayed in the presence and absence of YC-1 (Cayman Chemical) at a final concentration of 150 μM. The 1-NO form was made via addition of 50 μM DEA/NO to the protein and then removal of excess NO by three cycles of dilution and concentration using a 10K Ultrafree-0.5 centrifugal filter device (Millipore) into 50 mM HEPES (pH 7.4), containing 50 mM NaCl, and 1 mM DTT (*19*). Electronic absorption spectra of the samples were collected before each assay. Duplicate end point assays were then initiated by addition of 3 mM $MgCl_2$ and 1.5 mM GTP at 25 °C. Samples were quenched after 3 min by the addition of 400 μL of 125 mM $Zn(CH_3CO_2)_2$ and 500 μL of 125 mM Na_2CO_3. cGMP was quantified using a cGMP enzyme immunoassay kit, Format B (Biomol), per the manufacturer's instructions. All experiments were repeated two or three times to ensure reproducibility.

Resonance Raman and Electronic Absorption Spectroscopies. The xsNO sGC adduct for resonance Raman and electronic absorption studies was prepared via anaerobic addition of ^{14}NO (or ^{15}NO)-saturated buffer [50 mM HEPES (pH 7.4), containing 50 mM NaCl, and 1 mM DTT] to ligand-free sGC under an argon atmosphere. The final NO concentration was ∼150 μM. The 1-NO sGC adduct was prepared from the excess NO-bound sample via three cycles of dilution and concentration with NO-free buffer using a 10K Ultrafree-0.5 centrifugal filter device (Millipore). YC-1- or BAY 41-2272-bound samples were prepared via anaerobic addition of stock solutions (in DMSO) of respective effectors to the NO-bound sample. The final YC-1 concentration was 100−150 μM [∼2% (v/v) DMSO]. The final concentration of BAY 41-2272 (Sigma) was 15 μM [∼2% (v/v) DMSO]. The final protein concentration was 4−10 μM.

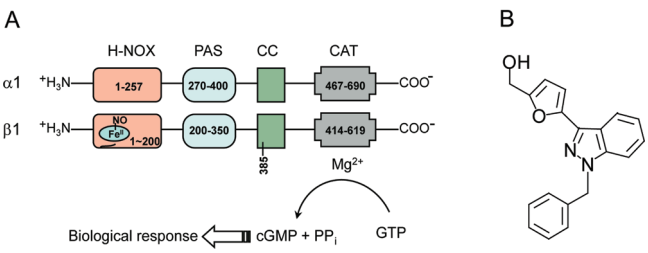

FIGURE 1: (a) Domain structure of sGC (adapted from ref *4*). (b) Structure of YC-1.

RR spectra were recorded via backscattering geometry at room temperature. The excitation wavelength of 400 nm was obtained by frequency doubling, using a nonlinear lithium triborate crystal, of a Ti:sapphire laser (Photonics International TU-UV), which was pumped by the second harmonic of a Q-switched Nd:YLF laser (Photonics Industries International, GM-30-527). The laser power at the sample was kept to a minimum (< 1 mW) by using a cylindrical lens to avoid the photolysis of bound NO. Scattered light was collected and focused onto a single spectrograph (SPEX 1269, 3600 grooves/mm) equipped with a CCD detector (Roper Scientific) operating at −110 °C. Spectra were calibrated with dimethylformamide and DMSO and analyzed with Grams A/I (Thermo-Galactic). UV−visible spectra were recorded on the Agilent 8453 UV−visible spectrophotometer (Agilent Technologies) and processed using Grams A/I.

Density Functional Theory (*DFT*) *Calculations*. DFT calculations on the 5-c Fe(II)NO porphine model complex were performed using Gaussian 03 (*23*). The standard 6-31G* basis set was used for all the atoms except Fe, for which Ahlrichs' valence triple-ζ (VTZ) basis set was chosen (*24*). All calculations were performed assuming a doublet ground state. The unrestricted nonhybrid DFT functional, UBLYP, was employed, with an ultrafine integration grid. The structures with the fixed FeNO angle at specific values were optimized using tight convergence criteria and C_s symmetry constraints, which kept the NO ligand in the plane bisecting the Fe−N(pyrrole) bonds. Vibrational frequencies were then calculated and taken directly from the Gaussian program without scaling.

RESULTS

NO Adduct Spectra. Full-length sGC and N-terminal truncations of the β1 subunit [β1(1−385) and β1(1−194)] were used in this study (Figure 1). The domain structure of sGC is illustrated in Figure 1. The β1(1−194) truncation contains the H-NOX domain with the heme ligated by His105 (*22*). β1(1−385) contains the H-NOX, PAS, and part of the CC (coiled-coil) domains (*25*). β1(1−385) forms a homodimer (*26*), and β1(1−194) is a monomer (*22*). Three homologous bacterial H-NOX domain structures have been published (*7*, *27*−*29*), and Figure 2 shows a homology model for the sGC H-NOX domain based on the *Tt* H-NOX structure (*7*). We examined the effect of residue substitution in the putative distal heme-binding pocket, I145Y, and in the putative

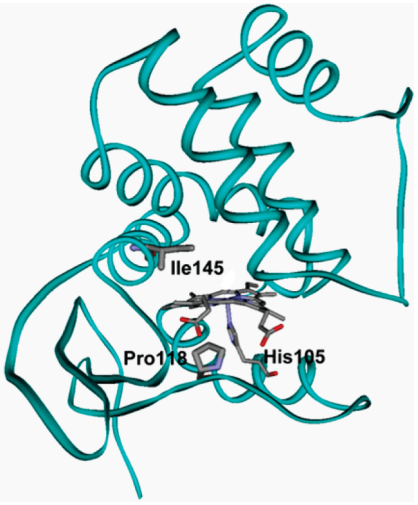

FIGURE 2: Homology model of the sGC β1 H-NOX domain [based on *Tt* H-NOX structure (PDB entry 1U55)].

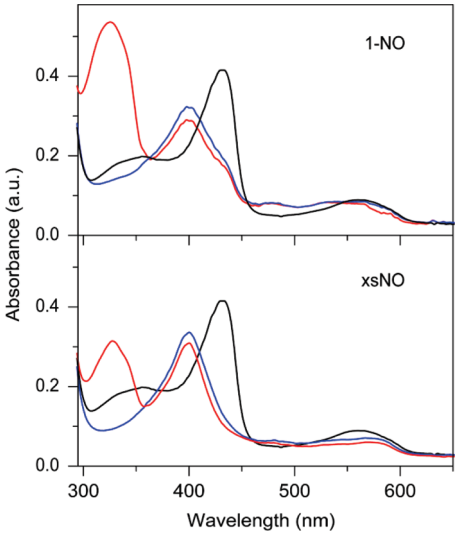

FIGURE 3: UV−visible spectra of ligand-free (black), NO-bound (blue), and NO- and YC-1-bound (red) full-length WT sGC. Effects of 1-NO (top) and xsNO (bottom) binding are shown. Absorption at 326 nm is due to YC-1.

proximal heme-binding pocket, P118A (Figure 2), on the binding of NO to β1(1−194).

All wild-type (WT) and β1 mutants contained 5-c Fe(II) heme, as evidenced by Soret absorption bands at ∼430 nm (Figure 3; only full-length WT sGC spectra are shown), and ν_{Fe-His} RR bands at 205−215 cm^{-1} (not shown). NO binding induced the breakage of the proximal Fe−His bond, producing 5-c NO-heme, with ∼400 nm Soret absorption bands (Figure 3) and ∼520 and ∼1680 cm^{-1} RR bands (Figures 4 and 5). These RR bands are associated with Fe−NO and N−O stretching vibrations of the bound NO and are sensitive to NO isotope substitution [see ^{14}NO − ^{15}NO difference spectra (Figure 4)]. As discussed elsewhere (*30*), the ∼520 cm^{-1} vibration is actually a mixture of Fe−N stretching and Fe−N−O bending coordinates, resulting from the bent Fe−N−O geometry. However, this mode responds to changes in backbonding similar to the Fe−CO stretching vibrations of corresponding CO adducts (*30*) and is designated ν_{FeN} for the sake of simplicity.

1-NO and xsNO Adducts. sGC activity associated with NO bound only at the heme (1-NO) and excess NO (xsNO) is shown

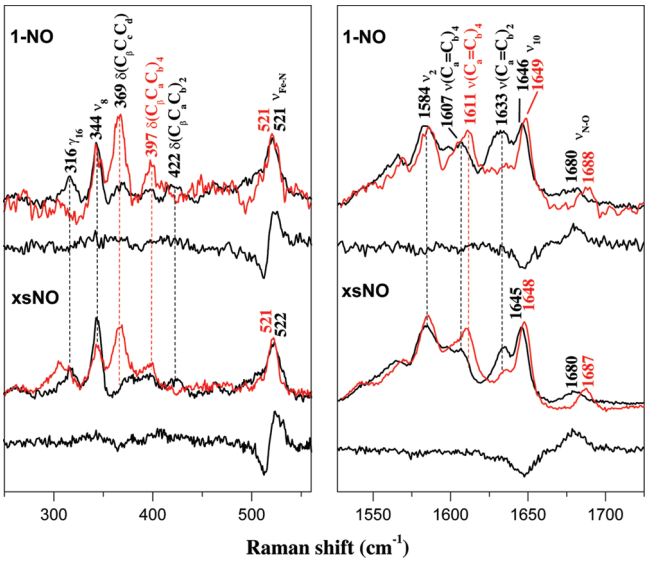

FIGURE 4: 400 nm-excited RR spectra of full-length WT sGC containing one NO (1-NO), excess NO (xsNO), and the ^{14}NO − ^{15}NO difference bands (black), and with added YC-1 (red). Band assignments and frequencies are indicated. Full spectra are given in Figure S1 of the Supporting Information.

in Table 1. Excess NO can be removed by dialysis, allowing spectral comparison of the two forms, 1-NO and xsNO. The electronic absorption spectra were the same for the 1-NO and xsNO forms as expected on the basis of previous results (Figure 3) (*12*, *21*). There is a small fraction of unligated protein present in the 1-NO sample as indicated by the shoulder at ∼430 nm (Figure 3), and also by the 1358 cm^{-1} ν_4 RR band (Figure S1 of the Supporting Information). The RR spectra of the 1-NO and xsNO adducts were essentially identical (Figure 4 and Figure S1 of the Supporting Information). The ν_{NO} band was found at the same frequency, 1680 cm^{-1}, in the 1-NO and xsNO spectra, while the ν_{FeN} frequency was slightly higher, 522 vs 521 cm^{-1}, in the xsNO spectrum (Figure 4 and Table 2). The porphyrin vibrations were all at the expected positions for 5-c NO-heme (*8*, *31*), and the same in both spectra. The close similarity of the 1-NO and xsNO RR spectra establishes that binding of additional NO produced no significant structural alteration in the heme.

A subtle difference in the low-temperature EPR spectrum has been observed between 1-NO and xsNO samples, indicating that the NO-heme does sense the protein alteration induced by the additional NO interaction (*19*). However, this influence is not sufficient to alter the heme-NO vibrations significantly.

Effects of YC-1 Binding. The effector molecule YC-1 increases the basal activity of sGC ∼4-fold but enhances the activity of the 1-NO adduct much more, to ∼40-fold above the basal level (Table 1). In contrast, the effect of YC-1 on the activity of the xsNO adduct is small. The effect of YC-1 on the RR spectrum of the sGC−NO complex has not been thoroughly examined. Here, we find that the RR spectra of both the 1-NO and xsNO sGC adducts exhibit the following significant spectral changes after addition of YC-1 (Figure 4 and Figures S1 of the Supporting Information).

(1) In both cases, the ν_{NO} band shifts from ∼1680 to ∼1687 cm^{-1}; the ν_{FeN} band remains the same (521 cm^{-1}) for the 1-NO adduct and shifts back to 521 cm^{-1} for the xsNO adduct (Figure 4 and Table 2).

(2) The porphyrin ν_{10} band at ∼1645 cm^{-1} shifts up 3 cm^{-1} after addition of YC-1. This mode is sensitive to the heme

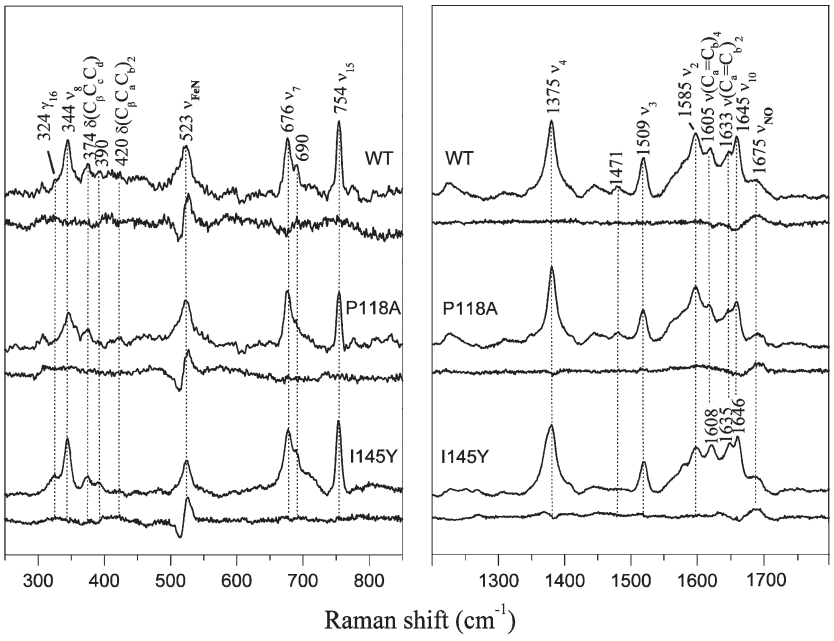

FIGURE 5: 400 nm-excited RR spectra of WT β1(1−194) with excess NO (xsNO) and of the P118A and I145Y variants. The $^{14}NO - {}^{15}NO$ difference bands are shown.

Table 1: Activation of sGC by Heme-Bound NO (1-NO), Additional NO (xsNO), and YC-1

	specific activity[a] (nmol min^{-1} mg^{-1})		fold activation	
sGC state	without YC-1	with YC-1	without YC-1	with YC-1
basal	8.4 ± 3.6	37 ± 11	1	4.4
1-NO	46 ± 2.3	325 ± 25	5.5	39
xsNO	1227 ± 375	1679 ± 536	146	200

[a]Determined in duplicate at 25 °C.

geometry, and an upshift suggests a reduction in the out-of-plane distortion of the 5-c heme-NO (*32*, *33*).

(3) YC-1 also induces intensity changes of RR bands associated with the 2- and 4-vinyl substituents on the heme (see Figure 6 for the labeling scheme), and also with a propionate bending mode at 369 cm^{-1} (*34*). There is a significant increase in the intensity of the 397 cm^{-1} band, assigned to bending of the 4-vinyl group, but intensity loss of the 422 cm^{-1} band, assigned to bending of the 2-vinyl group (*34*). At the same time, bands that can be assigned to the vinyl C=C stretches, at 1607 and 1633 cm^{-1} (*34*), gain and lose intensity, respectively, and the 1607 cm^{-1} band shifts up to 1611 cm^{-1}. The parallel with the 397 and 422 cm^{-1} intensity pattern suggests assignment of the 1607 and 1633 cm^{-1} pair to the 4- and 2-vinyl groups, respectively. The $\nu_{C=C}$ frequencies depend on the orientation of the vinyl groups relative to the pyrrole rings to which they are attached, in-plane orientations producing low values (*35*). The observed frequencies indicate that the 4-vinyl group lies in the plane of the pyrrole B ring (Figure 6) and rotates slightly out of the plane upon addition of YC-1. The 2-vinyl group is positioned out of the plane of the A ring, in the presence and absence of YC-1.

Increased RR intensity in the 4-vinyl modes implies increased resonance enhancement, reflecting greater displacement of the vibrational coordinates in the resonant $\pi-\pi^*$ excited state. This could result from the rotation of the 4-vinyl group toward the porphyrin plane or from a reduction in the degree of pyrrole tilting out of the porphyrin plane. The former mechanism is excluded if the 4-vinyl group starts out with an in-plane orientation, as inferred from the low $\nu_{C=C}$ frequency. Thus, we propose that pyrrole tilting is the mechanism of intensity modulation, and that the vinyl mode intensity pattern reflects pyrrole tilting toward and away from the porphyrin plane for rings B and A, respectively, to which the 4- and 2-vinyl groups are attached. Likewise, intensification of the 369 cm^{-1} propionate bending band likely involves tilting of pyrrole ring C and/or D toward the porphyrin plane. Additionally, the ν_{10} upshift indicates that the net out-of-plane displacement is reduced upon addition of YC-1. A similar RR spectrum was observed when BAY 41-2272 was added to the xsNO adduct (data not shown).

In summary, the binding of excess NO to sGC perturbs the heme minimally, but YC-1 binding produces the same significant structural changes in the heme conformation for both the 1-NO and xsNO adducts.

β1(1−194) and β1(1−385). RR spectra were also characterized for WT β1(1−194) (Figure 1), and for two mutants, P118A and I145Y (Figure 2). The P118A mutation was introduced to relieve nonbonded forces thought to be responsible for heme distortion in the homologous *Tt* H-NOX domain (*36*), while the I145Y mutation was introduced to test the effect of a potential H-bond donor to heme-bound ligands. The RR spectra of the NO adducts of the β1(1−194) mutants (Figure 5) were similar to the RR spectrum of the full-length sGC−Fe(II)-NO complex, except for slight up- and downshifts of ν_{FeN} and ν_{NO}, from 521 to 523 cm^{-1} and from 1680 to 1675 cm^{-1}, respectively (Table 2). Neither the P118A nor the I145Y substitution had any effect on the Fe(II)-NO RR spectra.

A similar RR spectrum was observed for β1(1−385) (Figure S2 of the Supporting Information and Table 2) which contains the PAS domain, and part of the coiled-coil domain, as well as the H-NOX domain (Figure 1). The minor variations observed were in ν_{FeN} and ν_{NO}, which had intermediate values, 522 and 1677 cm^{-1}, respectively, between the values observed for full-length sGC and β1(1−194).

FeNO Angle Dependence from DFT Computation. To investigate the origin of the YC-1-induced upshift of ν_{NO}, we

Table 2: Iron−Ligand Stretching Frequencies (cm^{-1}) for Various Full-Length and H-NOX Domain sGC−NO Complexes

		ν_{FeN} (cm^{-1})		ν_{NO} (cm^{-1})		
sGC	ligation	without YC-1	with YC-1	without YC-1	with YC-1	ref
full-length WT	xsNO	525		1677		*52*
	xsNO	521	521[a]	1681	1700[a]	*51*
	xsNO	522	521	1680	1687	tw[b]
	1-NO	521	521	1680	1688	tw[b]
β1(1−194) WT	xsNO	526		1677		*22*
	xsNO	523		1675		tw[b]
β1(1−194) P118A	xsNO	523		1675		tw[b]
β1(1−194) I145Y	xsNO	523		1675		tw[b]
β1(1−385) WT	xsNO	526		1676		*25*, *53*
	xsNO	522	522	1677	1677	tw[b]
	1-NO	522		1677		tw[b]

[a]In the presence of GTP and $MgCl_2$ (*51*). [b]This work.

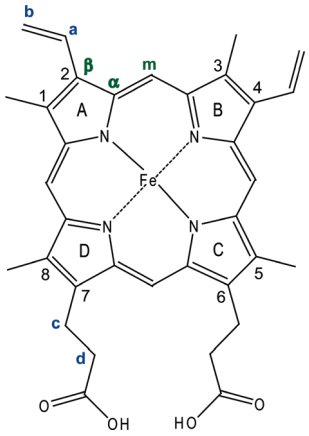

FIGURE 6: Labeling scheme for iron protoporphyrin IX (heme). Pyrrole C_α and C_β positions, as well as porphyrin C_m positions, are labeled green, while vinyl C_a and C_b and propionate C_c and C_d positions are labeled blue.

used density functional theory (DFT) to analyze the Fe−N−O angle dependence of the vibrational frequencies. A previous computation from our laboratory (*37*) had indicated that opening the Fe−N−O angle from its optimum value would elevate ν_{NO} with little effect on ν_{FeN}. We have revisited this computation, using a different density function method (BLYP instead of B3LYP), which was subsequently shown to give improved results for NO-heme adducts (*30*). Table 3 lists bond distances, vibrational frequencies, and relative energies for the model complex (NO)Fe(II)P (P = porphine), when the Fe−N−O angle was constrained to a range of values around the optimum, 142°. Figure 7 plots the computed frequencies and energies. Since the constrained structures are not at potential energy minima, the computed frequencies are not strictly correct, but the errors are small. However, DFT-computed frequencies are generally larger than experimentally observed ones because of systematic errors and the neglect of anharmonicity and solvent effects. Computed frequencies can generally be brought into agreement with experimental frequencies by empirical scaling of force constants associated with specific bond types (*38*−*40*). The ν_{FeN} and ν_{NO} frequencies computed for the optimum angle, 142.4°, can be brought into agreement with the values observed for the sGC−-NO complex using scale factors of 0.997 for N−O stretching and 0.870 for Fe−N stretching. The former value is in the range generally found with the BLYP functional for bonds between first-row atoms (*40*). For metal−ligand bonds, scaling factors have not been systematically analyzed, although in a Hartree−Fock study of metal−oxo stretches a scaling factor of 0.86 was obtained for first row transition metals (*41*).

The bending potential (Figure 7, inset) is fairly shallow. Opening or closing the Fe−N−O angle by 10° from the optimum decreases the energy (ΔE) by only ~1 kcal/mol. The bond distances vary monotonically with the Fe−N−O angle (Table 3). Specifically, as the angle opens up and approaches 180°, the Fe−N and N−O distances both decrease, reflecting the strengthening of the Fe−N and N−O bonds expected from Fe−NO backbonding. Consistent with this interpretation, the computed Mulliken charge on the O atom becomes steadily more negative, while the charge on the Fe becomes steadily more positive as the angle increases (Table S1 of the Supporting Information).

The ν_{FeN} and ν_{NO} frequencies likewise vary in concert for small angles (Figure 7), but as the angle exceeds the optimum value, ν_{FeN} levels off and begins to decline. The reason for this effect is that the effective mass of the NO group increases as the angle increases. At 180°, the effective mass is the full NO mass, while at 90°, it is only the mass of the N atom. This kinematic effect counters the force constant trend associated with decreasing Fe−N distance (*37*).

DISCUSSION

An essential finding of this study is that YC-1 and BAY 41-2272 significantly impact the heme structure of the sGC−NO complex, whereas excess NO does not, even though both serve to upregulate the relatively low activity of the sGC 1-NO adduct.

The effect of YC-1 on structure is evident in RR band intensity changes associated with the vinyl and propionate peripheral substituents on the heme. The changes suggest alterations in the degree of tilting of the pyrrole rings to which these substituents are attached. In addition, a YC-1-induced upshift of the conformation-sensitive ν_{10} band indicates that the net out-of-plane heme distortion is reduced.

The crystal structure of the *Tt* H-NOX domain, which is homologous to the heme-binding domain of sGC, reveals that the protein contains a highly distorted heme, with > 2 Å deviations of some atoms from the average plane, caused by a combination of ruffling and saddling distortions (*7*). The heme is held between distal and proximal subdomains of the protein. The crystal structure also revealed rotation of the two subdomains by

Table 3: DFT (BLYP) Structural Parameters (Å), Vibrational Frequencies (cm^{-1}), and Energies (kcal/mol) Calculated for the 5-c Fe(II)P-NO C_s Model at Varying Fe−N−O Angles

∠FeNO (deg)	Fe−NO	N−O	$Fe-N_p$	ν_{Fe-N}	ν_{N-O}	negative frequency	ΔE
120	1.7883	1.2065	2.010/2.036	1601	468	−	5.166
125	1.7641	1.2038	2.010/2.038	1621	512	−	3.093
130	1.7456	1.2014	2.011/2.040	1639	551	−	1.536
135	1.7313	1.1990	2.012/2.042	1658	578	−	0.530
140	1.7203	1.1969	2.014/2.043	1677	594	−	0.055
142.4	1.7159	1.1959	2.016/2.044	1686	599	−	0.000
145	1.7121	1.1948	2.017/2.044	1695	602	−	0.058
150	1.7058	1.1932	2.020/2.046	1710	602	−59	0.468
155	1.7009	1.1917	2.023/2.047	1724	599	−103	1.200
160	1.6985	1.1902	2.027/2.048	1738	591	−147	2.142
165	1.6970	1.1889	2.032/2.049	1749	582	−71/−187	3.154
170	1.6966	1.1879	2.037/2.049	1759	573	−158/−218	4.067
175	1.6972	1.1872	2.042/2.048	1766	565	−223/−238	4.703
180	1.6972	1.1870	2.045/2.045	1768	562	−244/−244	4.933

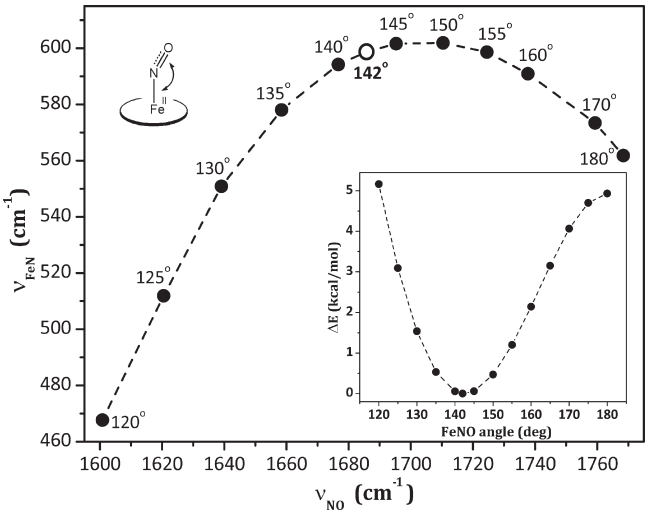

FIGURE 7: Computed frequencies for (NO)Fe(II)P when the Fe−N−O angle was constrained at the indicated values. The equilibrium angle is 142°. The inset shows computed energies associated with the angle constraints.

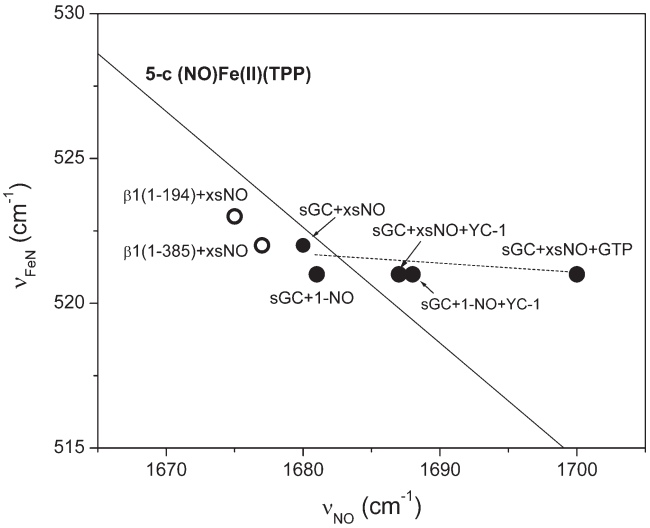

FIGURE 8: ν_{FeN}/ν_{NO} data for Fe(II) NO adducts of full-length (●) and truncated (○) wild-type sGC. The solid line is the correlation obtained from a series of 5-c (NO)Fe(II)TPP−X complexes (*50*).

∼11° between the two molecules in the unit cell. Moreover, replacement with Ala of a single residue, Pro115 (*Tt* H-NOX numbering), whose nonbonded contact with pyrrole ring D was predicted to be important in the distortion, resulted in significant relaxation of the heme, and displacement of the N-terminal (distal) subdomain of the protein (*36*). These results suggest that the coupling of heme distortion with segmental protein motion may be integral to the signaling mechanism in *Tt* H-NOX and, by extension, in sGC.

Tran et al. (*42*) reported that the heme relaxation in the P115A variant of *Tt* H-NOX was detectable in solution RR spectra. ν_{10} shifted to a higher frequency, as expected, and reduced intensity was observed for a number of bands in the 500−1000 cm^{-1} region, associated with pyrrole folding and methane C−H out-of-plane stretching modes. However, we found that mutation of the homologous proline to Ala in β1(1−194) (Pro118 in the rat β1 numbering system) had no effect on the RR spectrum of the sGC Fe(II)−NO complex. Likewise, mutation of Ile145 to Tyr, which introduces a Tyr into the heme distal pocket, was without effect. An sGC homology model based on *Tt* H-NOX puts β1 Ile145 in the same position as Tyr140 in *Tt* H-NOX. In *Tt* H-NOX, Tyr140 provides a stabilizing H-bond to the bound O_2. Mutation of Ile145 to Tyr in β1(1−385) enables the protein to bind O_2, suggesting that the tyrosine interacts with the heme ligand (*43*). The results here suggest that Tyr145 in β1(1−194) is not in an optimal position for H-bonding to the bound NO; however, kinetic studies comparing the interaction of NO, CO, and O_2 with β1(1−194), β1(1−385), and full-length sGC I145Y mutants will be important for evaluating the H-bonding capabilities of Tyr145 in the different proteins.

Although YC-1 induces a ν_{10} upshift in the sGC−NO RR spectrum, like the O_2-bound P115A substitution in *Tt* H-NOX, the other spectral changes are quite different in the two cases. The striking vinyl and propionate mode intensity changes induced by YC-1 are not seen in the *Tt* H-NOX P115A variant (*42*). Thus, simple relaxation of the heme geometry does not account for the YC-1 effect. Rather, there is an enforced geometry change, mediated by the peripheral substituents.

We note that YC-1 or BAY 41-2272 binding to the CO adduct of sGC also induces a high level of enzyme activity. Effects of YC-1 and BAY 41-2272 on CO adduct RR spectra have been documented in several studies (*44*−*47*), and vinyl and propionate RR mode changes very similar to those observed here for the NO

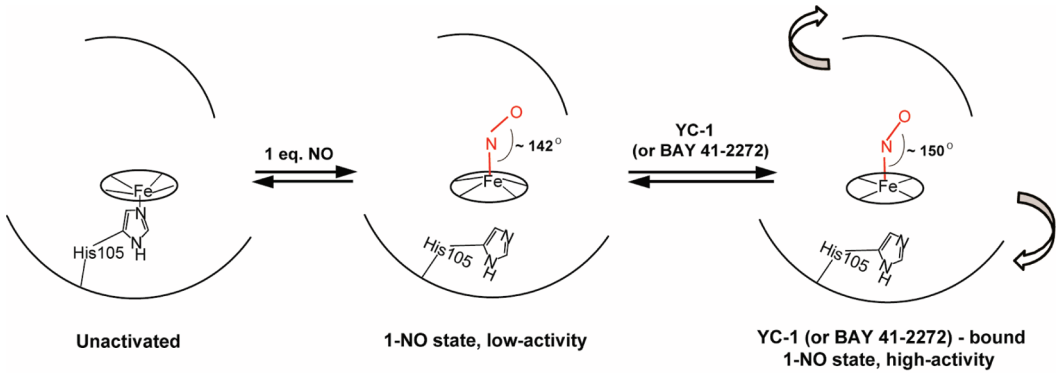

FIGURE 9: Structural model for activation-linked transitions of the sGC−NO complex. Binding of NO to the heme breaks the proximal Fe−His bond and induces porphyrin distortion via protein contacts. sGC exhibits a low level of activity in this state. Effector binding (YC-1 or BAY 41-2272) is suggested to induce an activating rotation of the two halves of the H-NOX domain, which alters the heme−protein contacts. In the altered conformation, the Fe−N−O angle is opened and pyrrole rings are rotated, producing net planarization of the heme. Binding of additional NO to the 1-NO adduct also induces high activity via an alternative mechanism that does not affect the heme-NO structure.

adduct have recently been reported (*48*, *49*). Thus, YC-1 and BAY 41-2272 are seen to activate both the NO and CO adducts by the same allosteric mechanism, which enforces pyrrole rotation and planarization of the heme.

An enforced geometry change is also indicated by the YC-1-induced upshift in ν_{NO}. We interpret this shift as resulting from an opening of the Fe−N−O angle, based on our DFT analysis. The primary determinant of the ν_{FeN} and ν_{NO} frequencies is backbonding from Fe to NO. Strengthening the backbonding, through inductive or electrostatic effects, increases ν_{FeN} while decreasing ν_{NO}. The resulting anticorrelation of the two frequencies is shown in Figure 8, in which the solid line represents the best fit to a series of 5-c (NO)Fe(II)TPP−X complexes, based on tetraphenylporphine with variable electron donating and withdrawing groups on the phenyl rings (*50*). The NO adducts of sGC are seen to fall on this line, but YC-1 moves the points off the line. An even larger deviation, in the same direction, is seen when GTP is added to the sGC−NO complex (Figure 8). GTP has been reported to shift ν_{NO} to 1700 cm^{-1}, again with no change in ν_{FeN} (*51*). In the previously published spectrum (*51*), one can see vinyl and propionate mode intensity changes similar to those we observe in the presence of YC-1 or BAY 41-2272. GTP is both a substrate and allosteric modulator of sGC, and preincubation of sGC with GTP converts the low-activity 1-NO form to a high-activity sGC state (*12*).

Our DFT analysis shows that opening the angle beyond its optimum of 142° increases ν_{NO} with little change in ν_{FeN}, because of countervailing force field and kinematic influences. According to Figure 7 and Table 3, opening the angle from 142 to 150° is expected to increase ν_{NO} by 24 cm^{-1}, the effect seen for GTP addition, while increasing ν_{FeN} by only 3 cm^{-1}. The energy required for this opening is small, 0.5 kcal/mol, and could be provided by nonbonded contacts with distal residues in the heme pocket when the protein undergoes a conformational change.

In summary, YC-1, BAY 41-2272, and GTP binding are inferred to induce protein conformational changes that alter the heme pocket, as illustrated in Figure 9. These changes enforce a slight opening of the Fe−N−O angle, and also pyrrole rotations leading to net planarization of the porphyrin, through peripheral nonbonded contacts with the vinyl and propionate substituents. We envision the conformational change as involving an activity-inducing rotation of the distal and proximal halves of the H-NOX domain.

These structural changes are not seen when excess NO is bound to sGC. There are no changes in the RR spectrum of the xsNO sGC adduct, relative to the 1-NO adduct, except for a very small upshift in ν_{FeN}. Thus, the profound effect of excess NO on enzyme activity is not accompanied by a significant alteration of the heme structure. Both YC-1 and excess NO produce major enhancements of the enzymatic rate, but the conformational changes underlying activation are clearly different.

SUPPORTING INFORMATION AVAILABLE

Complete ref *23*; Mulliken charges calculated for 5-c (NO)-Fe(II)P with varying Fe−N−O angles; RR spectra of full-length WT sGC containing one NO (1-NO), excess NO (xsNO), and the $^{14}NO - {}^{15}NO$ difference bands, covering the ν_4 and ν_7 regions; and RR spectra of β1(1−385) in the presence of 1-NO, xsNO, and YC-1. This material is available free of charge via the Internet at http://pubs.acs.org.

REFERENCES

1. Butler, A. R., and Williams, D. L. H. (1993) The physiological role of nitric oxide. *Chem. Soc. Rev. 22*, 233–241.
2. Tuteja, N., Chandra, M., Tuteja, R., and Misra, M. K. (2004) Nitric oxide as a unique bioactive signaling messenger in physiology and pathophysiology. *J. Biomed. Biotechnol. 4*, 227–237.
3. Bian, K., and Murad, F. (2003) Nitric oxide (NO): Biogeneration, regulation, and relevance to human diseases. *Front. Biosci. 8*, d264–d278.
4. Derbyshire, E. R., and Marletta, M. A. (2009) Biochemistry of soluble guanylate cyclase. In Handbook of Experimental Pharmacology (Schmidt, H. H. H. W., Hofmann, F., and Stasch, J.-P., Eds.) pp 17−31, Springer-Verlag, Berlin.
5. Kots, A. Y., Martin, E., Sharina, I. G., and Murad, F. (2009) A short history of cGMP, guanylyl cyclases, and cGMP-dependent protein kinases. In Handbook of Experimental Pharmacology (Schmidt, H. H. H. W., Hofmann, F., and Stasch, J.-P., Eds.) pp 1−14, Springer-Verlag, Berlin.
6. Boon, E. M., and Marletta, M. A. (2005) Ligand discrimination in soluble guanylate cyclase and the H-NOX family of heme sensor proteins. *Curr. Opin. Chem. Biol. 9*, 441–446.
7. Pellicena, P., Karow, D. S., Boon, E. M., Marletta, M. A., and Kuriyan, J. (2004) Crystal structure of an oxygen-binding heme domain related to soluble guanylate cyclases. *Proc. Natl. Acad. Sci. U.S.A. 101*, 12854–12859.
8. Yu, A. E., Hu, S., Spiro, T. G., and Burstyn, J. N. (1994) Resonance Raman spectroscopy of soluble guanylyl cyclase reveals displacement of distal and proximal heme ligands by NO. *J. Am. Chem. Soc. 116*, 4117–4118.
9. Stone, J. R., and Marletta, M. A. (1996) Spectral and kinetic studies on the activation of soluble guanylate cyclase by nitric oxide. *Biochemistry 35*, 1093–1099.

10. Wedel, B., Humbert, P., Harteneck, C., Foerster, J., Malkewitz, J., Bohme, E., Schultz, G., and Koesling, D. (1994) Mutation of His-105 in the β1 subunit yields a nitric oxide-insensitive form of soluble guanylyl cyclase. *Proc. Natl. Acad. Sci. U.S.A. 91*, 2592–2596.
11. Dierks, E. A., Hu, S., Yu, A., Spiro, T. G., and Burstyn, J. N. (1997) Demonstration of the role of scission of the proximal histidine-iron bond in the activation of soluble guanylyl cyclase through metalloporphyrin substitution studies. *J. Am. Chem. Soc. 119*, 7316–7323.
12. Russwurm, M., and Koesling, D. (2004) NO activation of guanylyl cyclase. *EMBO J. 23*, 4443–4450.
13. Cary, S. P. L., Winger, J. A., and Marletta, M. A. (2005) Tonic and acute nitric oxide signaling through soluble guanylate cyclase is mediated by nonheme nitric oxide, ATP, and GTP. *Proc. Natl. Acad. Sci. U.S.A. 102*, 13064–13069.
14. Fernhoff, N. B., Derbyshire, E. R., and Marletta, M. A. (2009) A nitric oxide/cysteine interaction mediates the activation of soluble guanylate cyclase. *Proc. Natl. Acad. Sci. U.S.A. 106*, 21602–21607.
15. Cary, S. P. L., Winger, J. A., Derbyshire, E. R., and Marletta, M. A. (2006) Nitric oxide signaling: No longer simply on or off. *Trends Biochem. Sci. 31*, 231–239.
16. Ko, F. N., Wu, C. C., Kuo, S. C., Lee, F. Y., and Teng, C. M. (1994) YC-1, a novel activator of platelet guanylate cyclase. *Blood 84*, 4226–4233.
17. Straub, A., Stasch, J.-P., Alonson-Alija, C., Benet-Buchholz, J., Ducke, B., Feurer, A., and Fürstner, C. (2001) NO-independent stimulators of soluble guanylate cyclase. *Bioorg. Med. Chem. Lett. 11*, 781–784.
18. Stasch, J.-P., and Hobbs, A. J. (2009) NO-independent, heme-dependent soluble guanylate cyclase stimulators. In Handbook of Experimental Pharmacology (Schmidt, H. H. H. W., Hofmann, F., and Stasch, J.-P., Eds.) pp 277−308, Springer-Verlag, Berlin.
19. Derbyshire, E. R., Gunn, A., Ibrahim, M., Spiro, T. G., Britt, R. D., and Marletta, M. A. (2008) Characterization of two different five-coordinate soluble guanylate cyclase ferrous−nitrosyl complexes. *Biochemistry 47*, 3892–3899.
20. Stasch, J. P., Becker, E. M., Alonso-Alija, C., Apeler, H., Dembowsky, K., Feurer, A., Gerzer, R., Minuth, T., Perzborn, E., Pleiss, U., Schroder, H., Schroeder, W., Stahl, E., Steinke, W., Straub, A., and Schramm, M. (2001) NO-independent regulatory site on soluble guanylate cyclase. *Nature 410*, 212–215.
21. Winger, J. A., Derbyshire, E. R., and Marletta, M. A. (2007) Dissociation of nitric oxide from soluble guanylate cyclase and heme-nitric oxide/oxygen binding domain constructs. *J. Biol. Chem. 282*, 897–907.
22. Karow, D. S., Pan, D., Davis, J. H., Behrends, S., Mathies, R. A., and Marletta, M. A. (2005) Characterization of functional heme domains from soluble guanylate cyclase. *Biochemistry 44*, 16266–16274.
23. Frisch, M. J. et al. (2004) Gaussian 03, revision E.01, Gaussian, Inc., Wallingford, CT.
24. Bauernschmitt, R., and Ahlrichs, R. (1996) Treatment of electronic excitations within the adiabatic approximation of time dependent density functional theory. *Chem. Phys. Lett. 256*, 454–464.
25. Schelvis, J. P. M., Zhao, Y., Marletta, M. A., and Babcock, G. T. (1998) Resonance Raman characterization of the heme domain of soluble guanylate cyclase. *Biochemistry 37*, 16289–16297.
26. Zhao, Y., and Marletta, M. A. (1997) Localization of the heme binding region in soluble guanylate cyclase. *Biochemistry 36*, 15959–15964.
27. Nioche, P., Berka, V., Vipond, J., Minton, N., Tsai, A. L., and Raman, C. S. (2004) Femtomolar sensitivity of a NO sensor from *Clostridium botulinum*. *Science 306*, 1550–1553.
28. Ma, X., Sayed, N., Beuve, A., and van den Akker, F. (2007) NO and CO differentially activate soluble guanylyl cyclase via a heme pivot-bend mechanism. *EMBO J. 26*, 578–588.
29. Erbil, W. K., Priceb, M. S., Wemmer, D. E., and Marletta, M. A. (2009) A structural basis for H-NOX signaling in *Shewanella oneidensis* by trapping a histidine kinase inhibitory conformation. *Proc. Natl. Acad. Sci. U.S.A. 106*, 19753–19760.
30. Ibrahim, M., Xu, C.-L., and Spiro, T. G. (2006) Differential sensing of protein influences by NO and CO vibrations in heme adducts. *J. Am. Chem. Soc. 128*, 16834–16845.
31. Decatur, S. M., Franzen, S., DePillis, G. D., Dyer, R. B., Woodruff, W. H., and Boxer, S. G. (1996) Trans effects in nitric oxide binding to myoglobin cavity mutant H93G. *Biochemistry 35*, 4939–4944.
32. Ma, J.-G., Zhang, J., Franco, R., Jia, S.-L., Moura, I., Moura, J. J. G., Kroneck, P. M., and Shelnutt, J. A. (1998) The structural origin of nonplanar heme distortions in tetraheme ferricytochrome c_3. *Biochemistry 37*, 12431–12442.
33. Indiani, C., de Sanctis, G., Neri, F., Santos, H., Smulevich, G., and Coletta, M. (2000) Effect of pH on axial ligand coordination of cytochrome c″ from *Methylophilus methylotrophus* and horse heart cytochrome c. *Biochemistry 39*, 8234–8242.
34. Hu, S., Smith, K. M., and Spiro, T. G. (1996) Assignment of protoheme resonance Raman spectrum by heme labeling in myoglobin. *J. Am. Chem. Soc. 118*, 12638–12646.
35. Marzocchi, M. P., and Smulevich, G. (2003) Relationship between heme vinyl conformation and the protein matrix in peroxidases. *J. Raman Spectrosc. 34*, 725–736.
36. Olea, C., Jr., Boon, E. M., Pellicena, P., Kuriyan, J., and Marletta, M. A. (2008) Probing the function of heme distortion in the H-NOX family. *ACS Chem. Biol. 3*, 703–710.
37. Coyle, C. M., Vogel, K. M., Rush, I., Thomas, S., Kozlowski, P. M., Williams, R., Spiro, T. G., Dou, Y., Ikeda-Saito, M., Olson, J. S., and Zgierski, M. Z. (2003) FeNO structure in distal pocket mutants of myoglobin based on resonance Raman spectroscopy. *Biochemistry 42*, 4896–4903.
38. Rauhut, G., and Pulay, P. (1995) Transferable scaling factors for density functional derived vibrational force fields. *J. Phys. Chem. 99*, 3093–3100.
39. Rauhut, G., Jarzecki, A. A., and Pulay, P. (1997) Density functional based vibrational study of conformational isomers: Molecular rearrangement of benzofuroxan. *J. Comput. Chem. 18*, 489–500.
40. Merrick, J. P., Moran, D., and Radom, L. (2007) An evaluation of harmonic vibrational frequency scale factors. *J. Phys. Chem. A 111*, 11683–11700.
41. Cundari, T. R., and Raby, P. D. (1997) Theoretical estimation of vibrational frequencies involving transition metal compounds. *J. Phys. Chem. A 101*, 5783–5788.
42. Tran, R., Boon, E. M., Marletta, M. A., and Mathies, R. A. (2009) Resonance Raman spectra of an O_2-binding H-NOX domain reveal heme relaxation upon mutation. *Biochemistry 48*, 8568–8577.
43. Boon, E. M., Huang, S. H., and Marletta, M. A. (2005) A molecular basis for NO selectivity in soluble guanylate cyclase. *Nat. Chem. Biol. 1*, 53–59.
44. Makino, R., Obayashi, E., Homma, N., Shiro, Y., and Hori, H. (2003) YC-1 facilitates release of the proximal his residue in the NO and CO complexes of soluble guanylate cyclase. *J. Biol. Chem. 278*, 11130–11137.
45. Li, Z., Pal, B., Takenaka, S., Tsuyama, S., and Kitagawa, T. (2005) Resonance Raman evidence for the presence of two heme pocket conformations with varied activities in CO-bound bovine soluble guanylate cyclase and their conversion. *Biochemistry 44*, 939–946.
46. Pal, B., and Kitagawa, T. (2005) Interactions of soluble guanylate cyclase with diatomics as probed by resonance Raman spectroscopy. *J. Inorg. Biochem. 99*, 267–279.
47. Martin, E., Czarnecki, K., Jayaraman, V., Murad, F., and Kincaid, J. R. (2005) Resonance Raman and infrared spectroscopic studies of high-output forms of human soluble guanylyl cyclase. *J. Am. Chem. Soc. 127*, 4625–4631.
48. Ibrahim, M., Derbyshire, E. R., Marletta, M. A., and Spiro, T. G. (2010) Probing soluble guanylate cyclase activation by CO and YC-1 using resonance Raman spectroscopy. *Biochemistry 49*, 3815–3823.
49. Pal, B., Tanaka, K., Takenaka, S., and Kitagawa, T. (2010) Resonance Raman spectroscopic investigation of structural changes of CO-heme in soluble guanylate cyclase generated by effectors and substrate. *J. Raman Spectrosc.* (in press).
50. Spiro, T. G., Ibrahim, M., and Wasbotten, I. H. (2008) CO, NO and O_2 as vibrational probes of heme protein active sites. In The smallest biomolecules: Diatomics and their interactions with heme proteins (Ghosh, A., Ed.) pp 96−123, Elsevier, Amesterdam.
51. Tomita, T., Ogura, T., Tsuyama, S., Imai, Y., and Kitagawa, T. (1997) Effects of GTP on bound nitric oxide of soluble guanylate cyclase probed by resonance Raman spectroscopy. *Biochemistry 36*, 10155–10160.
52. Deinum, G., Stone, J. R., Babcock, J. T., and Marletta, M. A. (1996) Binding of Nitric Oxide and Carbon Monoxide to Soluble Guanylate Cyclase As Observed with Resonance Raman Spectroscopy. *Biochemistry 35*, 1540–1547.
53. Denniger, J. W., Schelvis, J. P. M., Brandish, P. E., Zhao, Y., Babcock, G. T., and Marletta, M. A. (2000) Interaction of Soluble Guanylate Cyclase with YC-1: Kinetic and Resonance Raman Studies. *Biochemistry 39*, 4191–4198.